Available online at www.sciencedirect.com
ScienceDirect
Journal of Molecular Spectroscopy 245 (2007) 26–33
Journal of MOLECULAR SPECTROSCOPY
www.elsevier.com/locate/jms

Further spectroscopic investigations of the high energy electronic states of SrOH: The $\widetilde{B}'^2\Sigma^+(000)$–$\widetilde{A}^2\Pi(000)$ and the $\widetilde{D}^2\Sigma^+(000)$–$\widetilde{A}^2\Pi(000)$ transitions

J.-G. Wang [a,1], M.J. Dick [b], P.M. Sheridan [a,2], S. Yu [a], P.F. Bernath [a,b,*,1]

[a] Department of Chemistry, University of Waterloo, Waterloo, Ont., Canada N2L 3G1
[b] Department of Physics, University of Waterloo, Waterloo, Ont., Canada N2L 3G1

Received 23 May 2007; in revised form 19 June 2007
Available online 4 July 2007

Abstract

The $\widetilde{B}'^2\Sigma^+$ and $\widetilde{D}^2\Sigma^+$ states of SrOH were investigated using optical–optical double-resonance (OODR) spectroscopy. Rotational and fine structure parameters have been determined for these two states through a combined least-squares fit of the current OODR data along with the OODR data of the $\widetilde{C}^2\Pi$–$\widetilde{A}^2\Pi$ transition, the optical data of the $\widetilde{A}^2\Pi$–$\widetilde{X}^2\Sigma^+$ transition and the millimeter-wave pure rotational measurements of the $\widetilde{X}^2\Sigma^+$ state. The spin–rotation constant, γ, of the $\widetilde{B}'^2\Sigma^+$ state was found to be 0.002653 cm^{-1}, which is two orders of magnitude smaller than that of the $\widetilde{B}^2\Sigma^+$ state (−0.1447 cm^{-1}). This small γ value suggests that this state arises from a Sr^+ atomic orbital of mainly $6s\sigma$ character. This atomic orbital assignment is also supported by the large rotational constant observed in the $\widetilde{B}'^2\Sigma^+$ state and the similarity of the molecular constants to those of the $\widetilde{D}^2\Sigma^+$ state of CaOH. The rotational energy levels of the $\widetilde{D}^2\Sigma^+$state of SrOH were found to be largely perturbed, which prohibited the accurate determination of the spin–rotation constant in this state. This perturbation is most likely due to an interaction with a $^2\Sigma$ vibronic component of the nearby $\widetilde{C}^2\Pi$ state.

Keywords: SrOH; Optical–optical double-resonance; Alkaline-earth containing molecules

1. Introduction

Recently we have been conducting a series of high resolution spectroscopic investigations focusing on the high energy (>20 000 cm^{-1}) excited electronic states of CaOH and SrOH [1–3]. These states are of particular interest because the molecular geometry may differ from the linear configuration of the lower lying states. For example, extensive activity observed in the bending vibrational mode of the $\widetilde{F}^2\Pi$ state of CaOH has suggested a non-linear structure for this state [4]. These geometric changes may be the result of the different atomic orbital character of the unpaired electron in the higher energy states as compared to the lower lying states and vibronic interactions between states.

For SrOH, the low-lying $\widetilde{X}^2\Sigma^+$, $\widetilde{A}^2\Pi$, and $\widetilde{B}^2\Sigma^+$ states have been the subject of numerous detailed spectroscopic investigations [5–11], but studies of the higher energy states have been far more limited. The first observation of the higher energy electronic states of SrOH was reported by Beardah and Ellis [12,13]. In their work they used pulsed laser excitation spectroscopy to record moderate resolution spectra of transitions originating from the $^2\Sigma^+$ ground state to the $\widetilde{C}^2\Pi$, $\widetilde{D}^2\Sigma^+$, $\widetilde{E}^2\Sigma^+$, $\widetilde{F}^2\Pi$, and $\widetilde{B}'^2\Sigma^+$excited states in the range of 25 000–34 000 cm^{-1}. High-resolution measurements, however, are desirable to more precisely determine rotational and fine structure parameters for each of these high-lying electronic states. In turn this allows for a more detailed understanding of the electronic and geometric

* Corresponding author. Fax: +44 1904 432516.
E-mail address: pfb500@york.ac.uk (P.F. Bernath).
[1] Present address: Department of Chemistry, University of York, Heslington, York YO10 5DD, UK.
[2] Present address: Department of Chemistry and Biochemistry, Canisius College, Buffalo, NY 14208-1098, USA.

0022-2852/$ - see front matter © 2007 Elsevier Inc. All rights reserved.
doi:10.1016/j.jms.2007.06.005

structure of the molecule. To this end, we have recently applied the technique of optical–optical double-resonance (OODR) spectroscopy [14,15] to record high resolution spectra of the $\widetilde{C}^2\Pi$–$\widetilde{A}^2\Pi$ transitions of SrOH [2] and SrOD [3] and the $\widetilde{D}^2\Sigma^+$–$\widetilde{A}^2\Pi$ transition of CaOH [1]. Both the $\widetilde{D}^2\Sigma^+$ and $\widetilde{B}'^2\Sigma^+$ states of SrOH are excellent candidates for study by this method and are of particular interest for high resolution investigations. The $\widetilde{D}^2\Sigma^+$ state lies in a congested spectral region where many excited vibronic levels of the $\widetilde{C}^2\Pi$ state exist and the $\widetilde{B}'^2\Sigma^+$ state does not appear to have an equivalent state in the isolelectronic molecule, SrF.

In this paper, we present a high resolution study of the $\widetilde{B}'^2\Sigma^+$–$\widetilde{A}^2\Pi$ and the $\widetilde{D}^2\Sigma^+$–$\widetilde{A}^2\Pi$ transitions of SrOH using OODR spectroscopy. A least-squares fit that includes the assigned lines of each of these electronic transitions along with OODR data of the $\widetilde{C}^2\Pi$–$\widetilde{A}^2\Pi$ transition, the optical data of the $\widetilde{A}^2\Pi$–$\widetilde{X}^2\Sigma^+$ transition [6] and the millimeter-wave data of the $\widetilde{X}^2\Sigma^+$ state [10] has been performed. From this fit, more precise spectroscopic molecular constants for the $\widetilde{B}'^2\Sigma^+$ and $\widetilde{D}^2\Sigma^+$ states have been determined. The molecular structure and atomic orbital character of the $\widetilde{B}'^2\Sigma^+$ and $\widetilde{D}^2\Sigma^+$ states will be discussed based on the observed molecular parameters. In addition, the analysis of these data suggests that the $\widetilde{D}^2\Sigma^+$ state is severely perturbed, most likely by an excited vibronic component of the $\widetilde{C}^2\Pi$ state.

2. Experimental

A detailed description of the experimental apparatus and method used to synthesize SrOH in the gas phase has been given previously [2]. Briefly, Sr vapor was produced by resistively heating strontium metal in a graphite crucible using a Broida-type oven. The metal vapor was then entrained in a flow of argon carrier gas (1–5 Torr) and directed into the reaction region, where ~5 mTorr of concentrated hydrogen peroxide was introduced through a perforated ring above the crucible. A weak chemiluminescent flame due to the production of SrOH molecules was observed under optimal oven temperature and gas pressure conditions.

High-resolution spectra of the $\widetilde{B}'^2\Sigma^+$–$\widetilde{A}^2\Pi$ and the $\widetilde{D}^2\Sigma^+$–$\widetilde{A}^2\Pi$ transitions of SrOH were obtained using OODR spectroscopy. A linear cavity dye laser (~1 cm^{-1} band width), operating with DCM laser dye was used as the pump laser to excite the $\widetilde{A}^2\Pi_{1/2}$–$\widetilde{X}^2\Sigma^+$ or the $\widetilde{A}^2\Pi_{3/2}$–$\widetilde{X}^2\Sigma^+$ spin–orbit transitions of SrOH. The frequency of the pump laser was monitored using a Burleigh WA-2500 Wavemeter Jr. A Coherent 899-29 single-mode titanium–sapphire laser (nominal band width 10 MHz) was used as the probe laser to further excite the SrOH molecules from the intermediate $\widetilde{A}^2\Pi_{1/2}$ and $\widetilde{A}^2\Pi_{3/2}$ states to the high-lying $\widetilde{B}'^2\Sigma^+$ and $\widetilde{D}^2\Sigma^+$ electronic states. The pump and probe laser beams were focused colinearly into the reaction region above the Broida oven. The pump laser frequency was fixed to one of the band heads of the $\widetilde{A}^2\Pi$–$\widetilde{X}^2\Sigma^+$ transition while the probe laser was scanned. When the probe laser frequency corresponded to a transition between the rotational energy levels of the intermediate $\widetilde{A}^2\Pi$ state and an excited electronic state, the resulting UV fluorescence was observed using a photomultiplier tube (PMT). A 500 nm blue pass filter was placed in front of the PMT to eliminate fluorescence from the $\widetilde{A}^2\Pi$ state and laser scatter. Phase sensitive detection was employed by using a mechanical chopper to modulate the pump beam and a lock-in amplifier to process the fluorescence signal from the PMT. This further ensured that fluorescence signals observed in this experiment were only the result of the OODR excitation. Spectra were recorded in 5 cm^{-1} segments at a scan speed of 2 GHz per second with a data sampling interval of 20 MHz. The absolute frequency of the probe laser was determined by simultaneously recording the absorption spectrum of heated I_2 [16]. The continuity of the probe laser scan was monitored by recording simultaneously the 6-GHz Fabry–Perot fringes from the Coherent 899–29 wavemeter.

3. Results and analysis

The moderate-resolution study of SrOH by Beardah and Ellis [13] was used to determine the approximate frequency range to scan the probe laser in this investigation of the $\widetilde{B}'^2\Sigma^+$–$\widetilde{A}^2\Pi_{1/2}$ transition of SrOH. The top panel of Fig. 1 shows an overview of the high-resolution spectrum of the $\widetilde{B}'^2\Sigma^+$–$\widetilde{A}^2\Pi_{1/2}$ transition in the 11445–11480 cm^{-1} range. This spectrum exhibits a Hund's case (b)

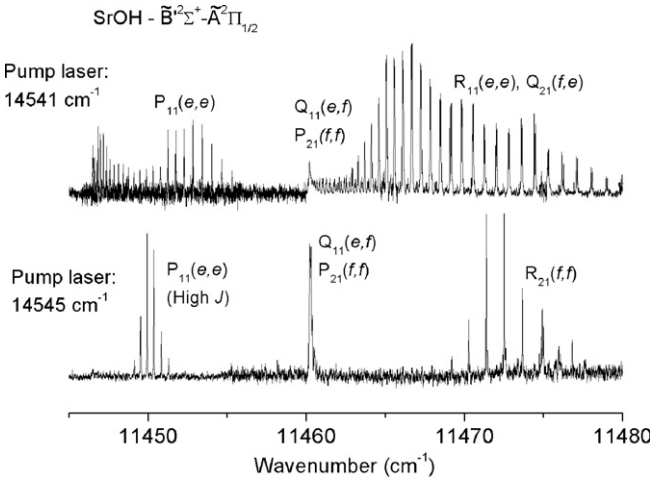

Fig. 1. Optical–optical double-resonance spectra of the $\widetilde{B}'^2\Sigma^+(000)$–$\widetilde{A}^2\Pi_{1/2}(000)$ transition of SrOH. In the top panel, the pump laser was tuned to the band heads of the $P_{11}(e,e)$ and $Q_{12}(e,f)$ branches of the $\widetilde{A}^2\Pi_{1/2}$–$\widetilde{X}^2\Sigma^+$ transition. As a result levels of e parity are predominantly populated in the intermediate state and subsequently the $P_{11}(e,e)$, $Q_{21}(f,e)$ and $R_{11}(e,e)$ branches of the $\widetilde{B}'^2\Sigma^+$–$\widetilde{A}^2\Pi_{1/2}$ transition are strongest. In the bottom panel, the pump laser has been tuned to the $Q_{11}(f,e)$ branch of the $\widetilde{A}^2\Pi_{1/2}$–$\widetilde{X}^2\Sigma^+$ system. Fewer lines are observed in this spectrum, however, the majority of the lines now arise from branches in which the lower rotational levels are of f parity. A few high J lines from the $P_{11}(e,e)$ branch are also present in the spectrum.

$^2\Sigma^+$–Hund's case (a) $^2\Pi$ transition branch structure [17]. In the top panel of Fig. 1, the pump laser frequency was fixed to the band heads of the $P_{11}(e,e)$ and $Q_{12}(e,f)$ branches ($\sim$14 541 cm^{-1}) of the $\widetilde{A}^2\Pi_{1/2}$–$\widetilde{X}^2\Sigma^+$ transition (e and f in parentheses denote the parities of the upper and lower state rotational levels, respectively). In this excitation scheme, the number of rotational (J) levels populated in the intermediate state is maximized. However, this pump laser frequency preferentially populated rotational levels with e parity in the intermediate $\widetilde{A}^2\Pi_{1/2}$ state and therefore the spectral lines with f parity in the intermediate state were quite weak. For this reason the $P_{11}(e,e)$, $Q_{21}(f,e)$, and $R_{11}(e,e)$ branches are predominantly observed in the upper panel of Fig. 1, while the $Q_{11}(e,f)$ $R_{21}(f,f)$, and $P_{21}(f,f)$ branches are present, but significantly weaker.

In an effort to more clearly observe transitions involving rotational levels with f parity in the intermediate state, the pump laser frequency was tuned to the higher wavenumber side of the $P_{11}(e,e)$ and $Q_{12}(e,f)$ band heads of the $\widetilde{A}^2\Pi_{1/2}$–$\widetilde{X}^2\Sigma^+$ transition. In this region, rotational transitions of the $Q_{11}(f,e)$ branch ($\sim$14 545 cm^{-1}) could be excited by the pump laser. The resulting overall spectrum is shown in the bottom panel of Fig. 1. The intensity of the $Q_{11}(e,f)$, $P_{21}(f,f)$, and $R_{21}(f,f)$ branches of the $\widetilde{B}'^2\Sigma^+$–$\widetilde{A}^2\Pi_{1/2}$ transition have increased significantly as compared to the upper panel of Fig. 1. As a result, an adequate number of spectral features originating from both parity components were observed to ensure a complete analysis of the $\widetilde{B}'^2\Sigma^+$–$\widetilde{A}^2\Pi$ transition.

For the $\widetilde{D}^2\Sigma^+$ state, the $\widetilde{A}^2\Pi_{3/2}$ spin–orbit component was used as the intermediate state. Initially, the pump laser frequency was fixed to the band heads of the $P_{21}(e,e)$ and $Q_{22}(e,f)$ branches ($\sim$14 803 cm^{-1}) of the $\widetilde{A}^2\Pi_{3/2}$–$\widetilde{X}^2\Sigma^+$ transition. From the previous moderate resolution work [12], the best estimate for the T_0 energy of the $\widetilde{D}^2\Sigma^+$ state was $\sim$27 698 cm^{-1}, and from this value the origin of the $\widetilde{D}^2\Sigma^+$–$\widetilde{A}^2\Pi_{3/2}$ transition was calculated to be $\sim$12 895 cm^{-1}. The upper panel of Fig. 2 shows lines from the $P_{12}(e,e)$, $R_{12}(e,e)$, and $Q_{22}(f,e)$ branches recorded over the range of 12 870–12 910 cm^{-1}. A comparison of this spectrum with the top panel of Fig. 1 indicates that the $\widetilde{D}^2\Sigma^+$–$\widetilde{A}^2\Pi_{3/2}$ transition does not appear to exhibit a similar structure. The $\widetilde{B}'^2\Sigma^+$–$\widetilde{A}^2\Pi_{1/2}$ spectrum has well defined branches and a clear band head in the $P_{11}(e,e)$ branch, while in contrast, the $\widetilde{D}^2\Sigma^+$–$\widetilde{A}^2\Pi_{3/2}$ spectrum exhibits a less well-defined branch structure, no clear band heads and no Q branch to mark the origin region. The absence of band heads in the $\widetilde{D}^2\Sigma^+$–$\widetilde{A}^2\Pi_{3/2}$ transition suggests that the rotational constants of the $\widetilde{D}^2\Sigma^+$ and $\widetilde{A}^2\Pi_{3/2}$ states are nearly identical. In an attempt to identify the remaining branches associated with the $\widetilde{D}^2\Sigma^+$–$\widetilde{A}^2\Pi_{3/2}$ transition, the frequency of the pump laser was tuned $\sim$5 cm^{-1} higher in energy than the band heads of the $P_{21}(e,e)$ and the $Q_{22}(e,f)$ branches of the $\widetilde{A}^2\Pi_{3/2}$–$\widetilde{X}^2\Sigma^+$ transition. This pump frequency ($\sim$14 808 cm^{-1}) corresponds to rotational transitions of the $Q_{21}(f,e)$ and $R_{22}(f,f)$ branches of the $\widetilde{A}^2\Pi_{3/2}$–$\widetilde{X}^2\Sigma^+$ spin–orbit component. The lower panel of Fig. 2 shows the simplified spectrum that was obtained using this pump frequency. The remaining branches ($Q_{12}(e,f)$ $P_{22}(f,f)$, and $R_{22}(f,f)$) are now clearly present.

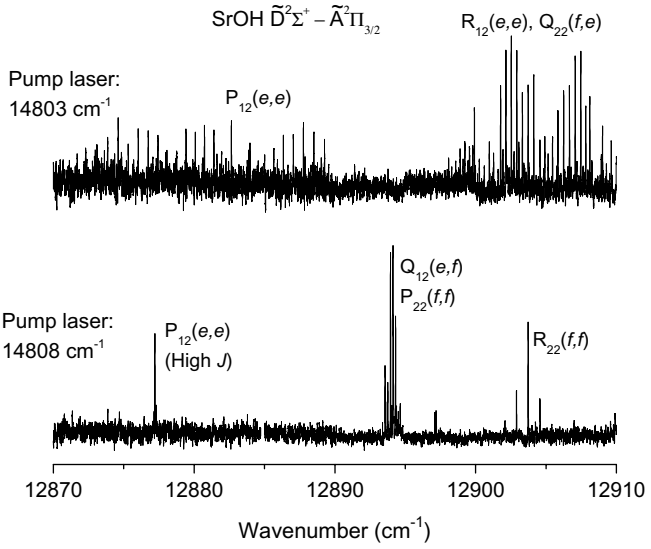

Fig. 2. Optical–optical double-resonance spectra of the $\widetilde{D}^2\Sigma^+(000)$–$\widetilde{A}^2\Pi_{3/2}(000)$ transition of SrOH. The top spectrum was measured with a pump laser wavenumber of 14803 cm^{-1}, which corresponds to the $Q_{22}(e,f)$ and $P_{21}(e,e)$ band heads in the $\widetilde{A}^2\Pi_{3/2}$–$\widetilde{X}^2\Sigma^+$ transition. As a consequence, levels of e parity are primarily populated in the intermediate state and only lines belonging to the $P_{12}(e,e)$, $R_{12}(e,e)$ and $Q_{22}(f,e)$ branches of the $\widetilde{D}^2\Sigma^+$–$\widetilde{A}^2\Pi_{3/2}$ transition appear in this spectrum. In the bottom spectrum the pump laser wavenumber has been tuned to 14 808 cm^{-1} and lines belonging to the $Q_{12}(f,e)$, $R_{22}(f,f)$ and $P_{22}(f,f)$ branches are now present.

In the previous moderate resolution study of SrOH by Beardah and Ellis [12] the assignment of the origin band of the $\widetilde{D}^2\Sigma^+$–$\widetilde{X}^2\Sigma^+$ was not completely secure. A strong band at $\sim$28 317 cm^{-1} was also suggested as a possibility for the $\widetilde{D}^2\Sigma^+(000)$–$\widetilde{X}^2\Sigma^+(000)$ transition. We also investigated the band at 28 317 cm^{-1} in the current OODR experiment. Using the same pump frequencies employed in the investigation of the $\widetilde{D}^2\Sigma^+$–$\widetilde{A}^2\Pi_{3/2}$ transition, the corresponding high resolution spectra of this system were obtained. The overall spectrum (pump frequency $\sim$14 803 cm^{-1}) for the 28 317 cm^{-1} system was exceptionally congested and covered a large spectral range ($\sim$80 cm^{-1}). This transition exhibited no clear band structure and when the pump laser frequency was set to $\sim$14 808 cm^{-1} there was no simplification of the spectrum as was observed for the $\widetilde{B}'^2\Sigma^+$–$\widetilde{A}^2\Pi$ transition. Branch assignments could not be made successfully for this system, which did not exhibit a Hund's case (b) $^2\Sigma^+$–Hund's case (a) $^2\Pi$ transition structure and without any other additional evidence we accept the original assignment of Beardah and Ellis [12].

For both the $\widetilde{B}'^2\Sigma^+ - \widetilde{A}^2\Pi_{1/2}$ and $\widetilde{D}^2\Sigma^+ - \widetilde{A}^2\Pi_{3/2}$ transitions, rotational assignments were made using the lower state combination differences of the $\widetilde{A}^2\Pi$ state [6–8]. For the $\widetilde{B}'^2\Sigma^+$–$\widetilde{A}^2\Pi_{1/2}$ transition, initially rotational assignments for the strong branches originating in e parity levels

of the $\widetilde{A}^2\Pi_{1/2}$ state were made. Branches originating in levels of f parity ($R_{21}(f,f)$, $Q_{11}(e,f)$, and $P_{21}(f,f)$) were then assigned using the spectrum in the lower panel of Fig. 1. A preliminary least-squares fit of these assigned rotational lines with the constants of the $\widetilde{A}^2\Pi$ state fixed to the previous results [6] was subsequently used to predict additional weak lines in all six branches. Using this method, a total of 225 rotational lines in these six branches were assigned for the $\widetilde{B}'^2\Sigma^+$–$\widetilde{A}^2\Pi_{1/2}$ transition. The measured lines are available as Supplementary material from this journal. For the $\widetilde{D}^2\Sigma^+$–$\widetilde{A}^2\Pi_{3/2}$ transition, rotational assignments were made in a similar manner. In total, 197 rotational lines from all six branches of the $\widetilde{D}^2\Sigma^+$–$\widetilde{A}^2\Pi_{3/2}$ transition were assigned and again the measured lines are available as Supplementary material from this journal.

Irregular line spacings were observed in several branches of the $\widetilde{D}^2\Sigma^+$–$\widetilde{A}^2\Pi_{3/2}$ transition. Fig. 3 shows a subsection of the $R_{12}(e,e)$ and $Q_{22}(f,e)$ branches of the $\widetilde{D}^2\Sigma^+$–$\widetilde{A}^2\Pi_{3/2}$ transition with rotational assignments, illustrating this spacing irregularity. In the $R_{12}(e,e)$ branch, a line spacing anomaly is observed around $J''=19.5$ and in the $Q_{22}(f,e)$ branch several more line spacing irregularities are found around $J''=23.5$ and $J''=25.5$. The odd spacings cause the relative line positions of the $R_{12}(e,e)$ and $Q_{22}(f,e)$ branches of the same J'' value to change around $J''=23.5$ (i.e. the energy of the two spin components for a given N' switches). Thus, below $J''=23.5$ the $Q_{22}(f,e)$ lines have a lower frequency than the $R_{12}(e,e)$ lines of the same J'', while above $J''=23.5$ the $Q_{22}(f,e)$ lines have a higher frequency than their same J'' $R_{12}(e,e)$ counterparts. This frequency alteration strongly suggests that the $\widetilde{D}^2\Sigma^+$ state is perturbed as the $\widetilde{A}^2\Pi_{3/2}$ state is known to be unperturbed.

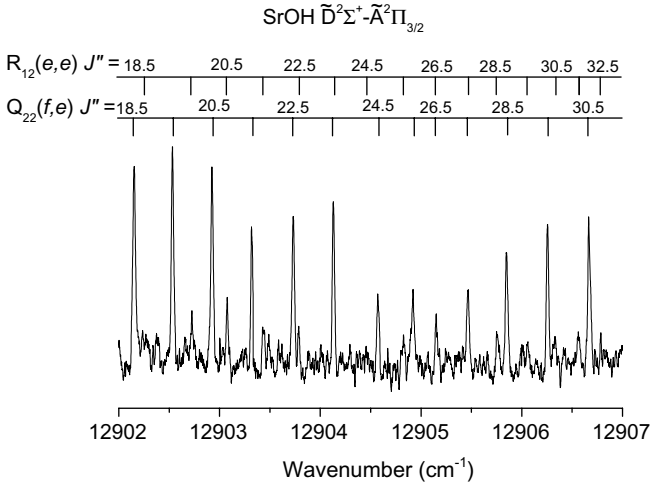

Fig. 3. An expanded portion of the OODR spectrum of the $\widetilde{D}^2\Sigma^+$–$\widetilde{A}^2\Pi_{3/2}$ transition of SrOH. J assignments of the $R_{12}(e,e)$ and $Q_{22}(f,e)$ are given on top of the spectrum. Severe irregularities in the line spacings of both the $Q_{22}(f,e)$ ($J''=25.5$) and $R_{12}(e,e)$ ($J''=19.5$) are clearly present. In addition, there is an alteration in the relative frequencies of lines of the same J'' value of the two branches at $J''=23.5$, suggesting the $\widetilde{D}^2\Sigma^+$ state is perturbed.

A least square fit of the measured line frequencies of the $\widetilde{B}'^2\Sigma^+$–$\widetilde{A}^2\Pi_{1/2}$ and $\widetilde{D}^2\Sigma^+$–$\widetilde{A}^2\Pi_{3/2}$ transitions to the Hund's case (b) $^2\Sigma^+$–Hund's case (a) $^2\Pi$ Hamiltonian of Brown [18] was performed. To minimize the uncertainties and determine the molecular parameters of the $\widetilde{B}'^2\Sigma^+$ and $\widetilde{D}^2\Sigma^+$ states more precisely, a global fit involving the majority of the previously recorded SrOH high-resolution data was performed. Therefore, the fit also included 38 pure rotational transitions measured in the millimeter-wave study of the $\widetilde{X}^2\Sigma^+(000)$ state [10], 585 lines recorded for the $\widetilde{A}^2\Pi(000)$–$\widetilde{X}^2\Sigma^+(000)$ transition [6], 454 assigned lines measured in the OODR study of the $\widetilde{C}^2\Pi(000)$–$\widetilde{A}^2\Pi(000)$ transition [2] and the current OODR measurements for the $\widetilde{B}'^2\Sigma^+(000)$–$\widetilde{A}^2\Pi_{1/2}(000)$ and $\widetilde{D}^2\Sigma^+(000)$–$\widetilde{A}^2\Pi_{3/2}(000)$ transitions. Each data set was weighted according to its experimental uncertainty. For the pure rotational and $\widetilde{A}^2\Pi(000)$–$\widetilde{X}^2\Sigma^+(000)$ transition data estimated uncertainties of $10^{-6}\,\mathrm{cm}^{-1}$ and $0.005\,\mathrm{cm}^{-1}$ were employed, respectively. The uncertainty of the OODR measurements was estimated to be $0.005\,\mathrm{cm}^{-1}$ except for weak or unresolved features, in which case an uncertainty of $0.01\,\mathrm{cm}^{-1}$ was used.

The spectroscopic constants for the electronic states of SrOH derived from the simultaneous fit are listed in Table 1. For comparison, the molecular parameters of the $\widetilde{B}^2\Sigma^+(000)$ [5] state are also presented in the table. For the $\widetilde{B}'^2\Sigma^+$ state, the band origin, T_0, ($26003.41015\,\mathrm{cm}^{-1}$) and rotational constant, B, ($0.2660963\,\mathrm{cm}^{-1}$) are similar to the results of Beardah and Ellis [13] ($T_0=25\,997\,\mathrm{cm}^{-1}$, $B=0.2658\,\mathrm{cm}^{-1}$), but are much more precisely determined. In this work, the spin–rotation constant, γ ($0.002653\,\mathrm{cm}^{-1}$) and the centrifugal distortion constant, D ($2.369\times10^{-7}\,\mathrm{cm}^{-1}$) have been determined for the first time.

Unfortunately, the fitting of the $\widetilde{D}^2\Sigma^+$–$\widetilde{A}^2\Pi_{3/2}$ transition data was not as straightforward. As mentioned previously, several of the observed branches showed irregular line spacings, most likely due to a perturbation in the $\widetilde{D}^2\Sigma^+$ state. These anomalies in the line spacings made it impossible to fit all 197 measured rotational lines of the $\widetilde{D}^2\Sigma^+$–$\widetilde{A}^2\Pi_{3/2}$ transition simultaneously. Any attempt at fitting all of the observed lines together resulted in an unusually large standard deviation in the fit. As a result several attempts were made to reduce the data set to obtain a consistent fit. In the end, a reasonable fit could only be achieved if the data set only included transitions with $J''<13.5$, as the most obvious irregularities in the line spacings all occur at higher J'' values. Therefore, the final data set included 65 rotational lines from all six observed branches of the $\widetilde{D}^2\Sigma^+$–$\widetilde{A}^2\Pi_{3/2}$ transition and the spectroscopic constants derived from this fit are listed in Table 1. Two rotational centrifugal distortion constants, D and H were required in the fit. The necessity of including two centrifugal distortion constants to fit a data set containing rotational lines of such low J values suggests that even transitions with $J''<13.5$ are affected by the perturbation.

Table 1
Spectroscopic Constants (in cm^{-1}) for SrOH[a,b]

Constant	$\widetilde{X}^2\Sigma^+(000)$	$\widetilde{A}^2\Pi(000)$	$\widetilde{B}^2\Sigma^+(000)$ [5]	$\widetilde{B}'^2\Sigma^+(000)$	$\widetilde{C}^2\Pi(000)$	$\widetilde{D}^2\Sigma^+(000)$[b]
T_0	0.0	14674.04177(42)	16377.505(1)	26003.41015(81)	27307.24760(69)	27701.6383(24)
B	0.249199813(12)	0.25378468(38)	0.25224(2)	0.2660963(21)	0.2546631(12)	0.25804 (10)
D	$2.17437(14)\times10^{-7}$	$2.16844(67)\times10^{-7}$	$2.15(3)\times10^{-7}$	$2.369(12)\times10^{-7}$	$2.1229(50)\times10^{-7}$	$38(12)\times10^{-7}$
H						$1.19(40)\times10^{-8}$
γ	$2.42748(31)\times10^{-3}$		−0.1447(3)	$2.653(31)\times10^{-3}$		0.01953(16)
A		263.58783(64)			24.6607(12)	
A_D		$1.330(26)\times10^{-5}$			$-2.285(12)\times10^{-4}$	
p		−0.143296(14)			−0.040743(79)	
p_D					$1.725(57)\times10^{-6}$	
q		$-1.534\ (19)\times10^{-4}$			$-5.9716(88)\times10^{-4}$	

[a] Values in parenthesis are 1σ standard deviations, in units of the last significant digits.
[b] The rotational constants for the $\widetilde{D}^2\Sigma^+$ state were derived from a fit that included only low J rotational lines ($J'' < 13.5$), see text.

4. Discussion

The low-lying electronic states of the alkaline-earth metal containing molecules are largely derived from the atomic orbital character of the unpaired electron on the metal atom [19,20]. For example, in SrOH the $\widetilde{X}^2\Sigma^+$ state arises mainly from the 5*s* atomic orbital on the strontium ion, while the first and second excited electronic states ($\widetilde{A}^2\Pi$ and $\widetilde{B}^2\Sigma^+$) are correlated to the 5*p* and 4*d* Sr^+ atomic orbitals. Theoretical calculations [21] based on a ligand field approach have sought to quantify the atomic orbital composition of the low-lying electronic states of SrOH. These calculations have determined that the atomic orbital character of the unpaired electron in the ground state is 80% 5*s* and 18% 5*p* in character. For the $\widetilde{A}^2\Pi$ state, a similar calculation concluded that this state is 58% 5*p* and 34% 4*d* in atomic orbital character, while the $\widetilde{B}^2\Sigma^+$ state was found to be 30% 5*p* and 53% 4*d* in character. The relative ratios of the atomic orbital character of the unpaired electron can affect the electronic and geometric properties of the molecule in an electronic state.

Unfortunately, there have been no theoretical calculations of the atomic orbital character of the unpaired electron in higher lying electronic states of SrOH. However, some information may be extracted from the spectroscopic constants in these states. For the $\widetilde{B}'^2\Sigma^+$ state, a comparison of the spin–rotation constant, γ, to those of the two lower energy $^2\Sigma^+$ states (Table 1) indicates that there is a similarity between the γ values of the $\widetilde{X}^2\Sigma^+(\gamma = 0.00242748\ cm^{-1})$ and the $\widetilde{B}'^2\Sigma^+(\gamma = 0.00265\ cm^{-1})$ states. The absolute value of the spin–rotation constants in the $\widetilde{X}^2\Sigma^+$ and $\widetilde{B}'^2\Sigma^+$ states is approximately 50 times smaller than that of the $\widetilde{B}^2\Sigma^+$ state. This suggests that the atomic orbital character of the $\widetilde{B}'^2\Sigma^+$ state is dominated by an orbital of $s\sigma$ character (6*s*σ), like the $\widetilde{X}^2\Sigma^+$ state (5*s*σ), rather than $p\pi$ character as for the $\widetilde{B}^2\Sigma^+$ state (4*p*π and 5*d*π). Electronic states arising from atomic orbitals of $s\sigma$ character do not usually interact with nearby electronic states and do not form unique perturber/pure precession pairs [22] with neighboring $^2\Pi$ states. In contrast, the $\widetilde{B}^2\Sigma^+$ state can interact with the $\widetilde{A}^2\Pi$ state, which results in the large value of γ for this state [22].

Further evidence for the $s\sigma$ character of the $\widetilde{B}'^2\Sigma^+$ (6*s*σ) state may be found by examining the Sr–O bond length. Table 2 lists the Sr–O and O–H bond lengths for the observed states of SrOH. For the $\widetilde{B}'^2\Sigma^+$ and $\widetilde{D}^2\Sigma^+$ states, the rotational constant has only been determined for one isotopologue, therefore, the O–H bond length was fixed to the ground state value. A comparison of the Sr–O bond lengths shows that this parameter is by far the shortest in the $\widetilde{B}'^2\Sigma^+$ state. This observation is consistent with the assumption that the $\widetilde{B}'^2\Sigma^+$ state arises from an atomic orbital significant in $s\sigma$ character. Orbitals of $s\sigma$ character are large and diffuse, allowing the negatively charged ligand (OH^-) to more closely approach the strontium ion and thereby form a shorter bond. The 6*s*σ orbital will be larger and more diffuse than the

Table 2
Bond lengths (Å) for SrOH

	$\widetilde{X}^2\Sigma^+$[a]	$\widetilde{A}^2\Pi$[b]	$\widetilde{B}^2\Sigma^+$[c]	$\widetilde{B}'^2\Sigma^+$[d]	$\widetilde{C}^2\Pi$[e]	$\widetilde{D}^2\Sigma^+$[f]
r_0(SrO)	2.111	2.091	2.098	2.041	2.096	2.073
r_0(OH)	0.922	0.922	0.921	0.922	0.822	0.922

[a] Determined from the millimeter-wave data of SrOH, SrOD, and ^{86}SrOH [10].
[b] Determined from the optical data of SrOH [6] and SrOD [3].
[c] Determined from the optical data of SrOH and SrOD [5].
[d] Determined from the optical–optical double-resonance data of SrOH [this work] and a fixed r_0 (OH) of 0.922 Å.
[e] Determined from the optical–optical double-resonance data of SrOH [2] and SrOD [3]. The anomalously short O–H separation in the $\widetilde{C}^2\Pi$ state of SrOH is either a reflection of a large amplitude bending motion in SrOH or more likely a consequence of an interaction of the state with a neighboring state.
[f] Determined from the optical–optical double-resonance data of SrOH [this work] and a fixed r_0 (OH) of 0.922 Å.

$5s\sigma$ orbital due to the higher principal quantum number, which allows for a shorter metal–ligand bond length in the $\widetilde{B}'^2\Sigma^+$ state than in the $\widetilde{X}^2\Sigma^+$ state. An investigation of the isotopologue SrOD is needed, however, to determine the OH and Sr–O bond lengths independently.

Additional evidence for the assignment of the $\widetilde{B}'^2\Sigma^+$ state of SrOH arising from an atomic orbital of predominantly $s\sigma$ character ($6s\sigma$) may be found by comparing the molecular properties of this state to those of an analogous state of another alkaline-earth metal containing molecule. A state equivalent to the $\widetilde{B}'^2\Sigma^+$ state of SrOH has not yet been observed in the isolelectronic molecule, SrF, however, such a state exists for CaOH. Fig. 4 shows a comparison of the energy ordering of the observed electronic states of CaOH to SrOH. The ordering is similar between these two molecules and specifically, the $\widetilde{D}^2\Sigma^+$ state of CaOH like the $\widetilde{B}'^2\Sigma^+$ state of SrOH, is the lowest of the higher energy ($>25000\ \mathrm{cm}^{-1}$) states of CaOH. Recently, the $\widetilde{D}^2\Sigma^+$ state of CaOH was studied at high-resolution [1] using OODR spectroscopy. From this investigation the $\widetilde{D}^2\Sigma^+$ state was found to have the smallest γ value of all the observed $^2\Sigma^+$ states and the shortest Ca–O bond length. Theoretical calculations showed that this state arises from the unpaired electron residing in the $5s\sigma$ atomic orbital on the calcium cation. These observations are consistent with the properties of the $\widetilde{B}'^2\Sigma^+$ state of SrOH and further suggest that this state arises from the $6s\sigma$ atomic orbital on the strontium atom.

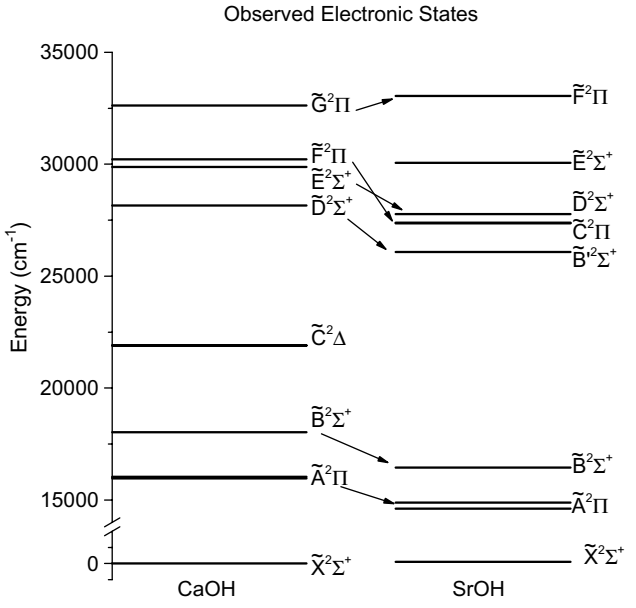

Fig. 4. An energy level diagram correlating the observed electronic states of CaOH with those of SrOH. The diagram suggests that the $\widetilde{B}'^2\Sigma^+$ state of SrOH is analogous to the $\widetilde{D}^2\Sigma^+$ state of CaOH. This assignment is supported by the similarity in the spectroscopic parameters of the two states. The $\widetilde{C}^2\Pi$ and $\widetilde{D}^2\Sigma^+$ of SrOH lie close in energy and appear to form a unique peturber/pure procession pair similar to the $\widetilde{A}^2\Pi$ and $\widetilde{B}^2\Sigma^+$ states of SrOH. Unfortunately, because of the perturbation of the $\widetilde{D}^2\Sigma^+$ state, these states cannot be conclusively classified as this type of pair.

Because the $\widetilde{B}'^2\Sigma^+$ state most likely arises from the $6s\sigma$ orbital of Sr^+, it is reasonable to conclude that the $\widetilde{C}^2\Pi$ and $\widetilde{D}^2\Sigma^+$ states of SrOH are largely derived from the $6p\pi$ Sr^+ atomic orbitals. In this case, these states likely form a pure precession/unique perturber pair [22]. In the recent OODR study of the $\widetilde{C}^2\Pi$ state of SrOH [2], this assumption and the energy separation from the $\widetilde{D}^2\Sigma^+$ state was used to estimate the Λ-doubling constants in the $\widetilde{C}^2\Pi$ state. A reasonable agreement between the experimental and theoretical Λ-doubling constants was found, which supported this assumption. Subsequently using this model, the spin–rotation constant, γ, for the $\widetilde{D}^2\Sigma^+$ state of SrOH can be estimated. According to the pure precession model and the unique perturber assumption, the spin–rotation constant in the $\widetilde{D}^2\Sigma^+$ state is given by the expression [22]:

$$\gamma = \frac{2A_{SO}B\ell(\ell+1)}{E(\widetilde{C}^2\Pi) - E(\widetilde{D}^2\Sigma^+)} \tag{1}$$

where B is the rotational constant,A_{SO} is the spin–orbit constant,ℓ is the atomic orbital angular momentum of the $^2\Pi$ state and E is the state energy.Using ℓ (effective) $= 1$ (assuming pure p character) and the values for the molecular constants listed in Table 1 ($A(\widetilde{C}^2\Pi) = 24.6607\ \mathrm{cm}^{-1}$, $B(\widetilde{D}^2\Sigma^+) = 0.25804\ \mathrm{cm}^{-1}$,$E(\widetilde{C}^2\Pi) = 27307.24760\ \mathrm{cm}^{-1}$,and $E(\widetilde{D}^2\Sigma^+) = 27701.6383\ \mathrm{cm}^{-1}$) γ is estimated to be about $-0.064\ \mathrm{cm}^{-1}$.A comparison of this value with the one derived for the $\widetilde{D}^2\Sigma^+$ state in the current global fit of the SrOH data ($\gamma = 0.01953\ \mathrm{cm}^{-1}$) shows a similarity in the magnitude of the two values,but a disagreement in the sign.According to Eq.(1),a change in the sign of the spin–rotation constant is only possible if the $\widetilde{C}^2\Pi$ lies below the $\widetilde{D}^2\Sigma^+$ states.However,from the energy ordering of the electronic states of SrOH (Fig.4) this is not the case and therefore,the inconsistency in the sign is most likely a reflection of the perturbation in the $\widetilde{D}^2\Sigma^+$ state mentioned previously.Another possibility that could explain the inconsistencies in the sign of the spin–rotation constants is that the $\widetilde{F}^2\Pi$ and$\widetilde{D}^2\Sigma^+$ states form the pure precession/unique perturber pair. However, this is unlikely due to the large energy separation between these two states.

One possibility for the cause of the perturbation in the $\widetilde{D}^2\Sigma^+$ state of SrOH is an interaction with a $^2\Sigma$ vibronic level of the $\widetilde{C}^2\Pi$ state that arises via Renner–Teller coupling as suggested by Beardah and Ellis [12]. For one quantum of the bending mode ($v_2 = 1$) in the $\widetilde{C}^2\Pi$ state, the term values for the two $^2\Sigma$ vibronic components are [23]

$$G(\kappa^2\Sigma) = T_0 + 2\omega_2\left(1 - \frac{1}{8}\varepsilon^2\right) + \frac{1}{2}A^*$$

$$G(\mu^2\Sigma) = T_0 + 2\omega_2\left(1 - \frac{1}{8}\varepsilon^2\right) - \frac{1}{2}A^*, \tag{2}$$

where T_0 is the electronic term value, ω_2 is the harmonic frequency of the bending vibration, ε is the Renner parameter and A^* is the effective spin–orbit coupling constant. The effective spin–orbit coupling constant is determined from A_{SO}, the true spin–orbit constant, ε, the Renner

parameter and ω_2, the bending frequency via the equation [23]

$$A^* = \sqrt{A_{SO}^2 + 4\varepsilon^2\omega_2^2}. \quad (3)$$

Unfortunately, precise measurements of the Renner–Teller parameter and the harmonic bending frequency for the $\widetilde{C}^2\Pi$ state have not yet been made. However, rough estimates of $\omega_2 \sim 255\ \mathrm{cm}^{-1}$ and $\varepsilon = 0.16$ have been reported by Beardah and Ellis [12]. Using these values and the spin–orbit constant of the $\widetilde{C}^2\Pi$ state ($24.6607\ \mathrm{cm}^{-1}$), the effective spin–orbit constant is calculated from Eq. (3) to be $A^* \sim 84\ \mathrm{cm}^{-1}$. Using $T_0 = 27307.24760\ \mathrm{cm}^{-1}$, the term values of the two vibronic $^2\Sigma$ components of the bending mode in the $\widetilde{C}^2\Pi$ state can then be calculated via Eq. (2): $G(\kappa^2\Sigma) \sim 27859\ \mathrm{cm}^{-1}$ and $G(\mu^2\Sigma) \sim 27774\ \mathrm{cm}^{-1}$. The upper vibronic component, $G(\kappa^2\Sigma) \sim 27859\ \mathrm{cm}^{-1}$, is much higher in energy than the observed $\widetilde{D}^2\Sigma^+(000)$ state ($27701.6383\ \mathrm{cm}^{-1}$). However, the lower vibronic component $G(\mu^2\Sigma) \sim 27774\ \mathrm{cm}^{-1}$ lies only approximately $72\ \mathrm{cm}^{-1}$ higher in energy than the observed $\widetilde{D}^2\Sigma^+(000)$ state. This $^2\Sigma$ vibronic state obeys Hund's case (a) coupling and has an estimated γ value of approximately $2B$ ($\sim 0.47\ \mathrm{cm}^{-1}$) [24].

Considering the uncertainties in the estimated values of ω_2 and ε, there is a strong likelihood that the lower vibronic $^2\Sigma$ component of the $\widetilde{C}^2\Pi$ state is the source of the perturbation in the $\widetilde{D}^2\Sigma^+(000)$ state. In addition, the difference in the magnitude between the estimated γ value for the $(\mu^2\Sigma)$ vibronic component and the value determined for the $\widetilde{D}^2\Sigma^+(000)$ state ($\gamma = 0.01953\ \mathrm{cm}^{-1}$) eliminates the possibility that the state observed in this study is a vibronic component of the $\widetilde{C}^2\Pi$ state. The sign and magnitude of γ for the $\widetilde{D}^2\Sigma^+(000)$ are consistent with a perturbation between the $\widetilde{C}^2\Pi$ and $\widetilde{D}^2\Sigma^+$ states. A mixing of the $(\mu^2\Sigma)$ vibronic component of the $\widetilde{C}^2\Pi$ state and the $\widetilde{D}^2\Sigma^+$ would be sufficient to switch the sign of the observed spin–rotation constant of the $\widetilde{D}^2\Sigma^+$ state from negative to positive. Additional studies will be necessary to confirm this possibility for the identity of the perturbing state. It would be of great interest to examine the $\widetilde{D}^2\Sigma^+$ state of the SrOD isotopologue to confirm the identity of the $\widetilde{D}^2\Sigma^+$ state and to observe how the perturbation changes as the bending frequency of the $\widetilde{C}^2\Pi$ state and the location of the electronic states differ for this isotopologue.

5. Conclusion

High resolution spectra of the $\widetilde{B}'^2\Sigma^+(000)$–$\widetilde{A}^2\Pi_{1/2}(000)$ and $\widetilde{D}^2\Sigma^+(000)$–$\widetilde{A}^2\Pi_{3/2}(000)$ transitions of SrOH have been recorded using optical–optical double-resonance spectroscopy. The observed frequencies of the rotational lines were fitted in combination with the optical data of the $\widetilde{A}^2\Pi(000)$–$\widetilde{X}^2\Sigma^+(000)$ [6] transition and the millimeter-wave pure rotational data of the $\widetilde{X}^2\Sigma^+$ state [10]. Rotational and fine structure constants have been determined for the $\widetilde{B}'^2\Sigma^+$ and $\widetilde{D}^2\Sigma^+$ states. The dominant atomic orbital character of the $\widetilde{B}'^2\Sigma^+$ state has been proposed to be $6s\sigma$ based on its small spin–rotation constant and short Sr–O bond length. This atomic orbital character assignment is consistent with that of the $\widetilde{D}^2\Sigma^+$ state of CaOH [1], which appears to be analogous to the $\widetilde{B}'^2\Sigma^+$ state of SrOH. A perturbation in the $\widetilde{D}^2\Sigma^+$ state of SrOH has most likely reversed the relative energy ordering of the e and f parity rotational levels below $J = 23.5$ in this state. Because little is known about the perturbing state, it is impossible to conclusively determine a value for the spin–rotation constant for the $\widetilde{D}^2\Sigma^+$ state, which in turn prohibited determining if the $\widetilde{C}^2\Pi$ and $\widetilde{D}^2\Sigma^+$ states form a pure procession/unique perturber pair. Based on estimates of the vibronic parameter the lower $^2\Sigma$ vibronic level of the first bending mode of the $\widetilde{C}^2\Pi$ state arising from Renner–Teller coupling is a strong candidate as the perturber of the $\widetilde{D}^2\Sigma^+$ state.

Acknowledgment

Financial support for this work was provided by the Natural Sciences and Engineering Research Council (NSERC) of Canada.

Appendix A. Supplementary data

Supplementary data for this article are available on ScienceDirect (www.sciencedirect.com) and as part of the Ohio State University Molecular Spectroscopy Archives (http://msa.lib.ohio-state.edu/jmsa_hp.htm).

References

[1] M.J. Dick, P.M. Sheridan, J.-G. Wang, S. Yu, P.F. Bernath, J. Mol. Spectrosc. 240 (2006) 238–243.
[2] J.-G. Wang, P.M. Sheridan, M.J. Dick, P.F. Bernath, J. Mol. Spectrosc. 236 (2006) 21–28.
[3] S. Yu, J.-G. Wang, P.M. Sheridan, M.J. Dick, P.F. Bernath, J. Mol. Spectrosc. 240 (2006) 26–31.
[4] R. Pereira, D.H. Levy, J. Chem. Phys. 105 (1996) 9733–9739.
[5] J. Nakagawa, R.F. Wormsbecher, D.O. Harris, J. Mol. Spectrosc. 97 (1983) 37–64.
[6] C.R. Brazier, P.F. Bernath, J. Mol. Spectrosc. 114 (1985) 163–173.
[7] P.I. Presunka, J.A. Coxon, J. Chem. Phys. 101 (1994) 201–222.
[8] P.I. Presunka, J.A. Coxon, Chem. Phys. 190 (1995) 97–111.
[9] P.I. Presunka, J.A. Coxon, Can. J. Chem. 71 (1993) 1689–1705.
[10] M.A. Anderson, W.L. Barclay Jr., L.M. Ziurys, Chem. Phys. Lett. 196 (1992) 166–172.
[11] T.C. Steimle, D.A. Fletcher, K.Y. Jung, C.T. Scurlock, J. Chem. Phys. 96 (1992) 2556–2564.
[12] M.S. Beardah, A.M. Ellis, J. Chem. Phys. 110 (1999) 11244–11254.
[13] M.S. Beardah, A.M. Ellis, J. Mol. Spectrosc. 218 (2003) 80–84.
[14] P.F. Bernath, R.W. Field, J. Mol. Spectrosc. 82 (1980) 339–347.
[15] C. Nitsch, J.O. Schröder, W.E. Ernst, Chem. Phys. Lett. 148 (1988) 130–135.
[16] S. Gerstenkorn J. Verges J. Chevillard, Atlas du Spectre d'Absorption de la Molecule d'Iode" Laboratoire Aimé Cotton, CNRS II 91405 Orsay France, 1982.
[17] G. Herzberg, Molecular Spectra and Molecular Structure Vol. I–Spectra of Diatomic Molecules, Krieger Publishing Company, Malabar, 1950.
[18] J.M. Brown, E.A. Colbourn, J.K.G. Watson, F.D. Wayne, J. Mol. Spectrosc. 74 (1979) 294–318.
[19] P.F. Bernath, Adv. Photochem. 23 (1997) 1–62.

[20] A.M. Ellis, Int. Rev. Phys. Chem. 20 (2001) 551–590.
[21] A.R. Allouche, M. Aubert-Frécon, J. Mol. Spectrosc. 163 (1994) 599–603.
[22] H. Lefebvre-Brion, R.W. Field, The Spectra and Dynamics of Diatomic Molecules, Elsevier, Amsterdam, 2004.
[23] G. Herzberg, Molecular Spectra and Molecular Structure Vol. III-Electronic Spectra and Electronic Structure of Polyatomic Molecules, Krieger Publishing Company, Malabar, 1991.
[24] J.T. Hougen, J. Chem. Phys. 36 (1962) 519–534.